MODELLING LONG-TERM EVOLUTION OF CEMENTITIOUS MATERIALS USED IN WASTE DISPOSAL

D. JACQUES[1]*, J. PERKO*, S. SEETHARAM*, D. MALLANTS**, J. GOVAERTS*

*Belgian Nuclear Research Centre (SCK•CEN), Institute for Environment, Health, and Safety, Mol, Belgium.

**CSIRO Land and Water, Waite Road - Gate 4, Glen Osmond SA 5064, Australia.

Abstract

This report summarizes the latest developments at SCK•CEN in modelling long-term evolution of cementitious materials used as engineered barriers in waste disposal. In a first section chemical degradation of concrete during leaching with rain and soil water types is discussed. The geochemical evolution of concrete thus obtained forms the basis for all further modelling. Next we show how the leaching model is coupled with a reactive transport module to determine leaching of cement minerals under diffusive or advective boundary conditions. The module also contains a simplified microstructural model from which hydraulic and transport properties of concrete may be calculated dynamically. This coupled model is simplified, i.e. abstracted prior to being applied to large-scale concrete structures typical of a near-surface repository. Both the original and simplified models are then used to calculate the evolution of hydraulic, transport, and chemical properties of concrete. Characteristic degradation states of concrete are further linked to distribution ratios that describe sorption onto hardened cement via a linear and reversible sorption process. As concrete degrades and pH drops the distribution ratios are continuously updated. We have thus integrated all major chemical and physical concrete degradation processes into one simulator for a particular scale of interest. Two simulators are used: one that can operate at relatively small spatial scales using all process details and another one which simulates concrete degradation at the scale of the repository but with a simplified cement model representation.

1. MODELLING CHEMICAL DEGRADATION OF CONCRETE DURING LEACHING WITH RAIN AND SOIL WATER TYPES

1.1. Introduction

Cement and concrete are typically not in thermodynamic equilibrium with the surroundings in which they are located. Because concrete used in e.g. waste conditioning and surface disposal is not an isolated system, water infiltration and solute migration from the surrounding environment will alter the concrete pore water and solid phase composition. As a result, the solubility and sorption of contaminants will change too (see Wang et al. [1] for an extensive review of sorption values for radionuclides and chemically toxic elements as function of the cement degradation state).

While concrete degradation usually occurs as the result of a combination of physical, mechanical, and chemical processes, this paper emphasizes the role of chemical degradation. Typical chemical degradation reactions are decalcification, dissolution and leaching of cement components and carbonation (Glasser et al. [2]), amongst others. These reactions induce a gradual change in the pore water composition, from typical "young" concrete pore water with a pH above 13 to more evolved pore water with a pH lower than 10. Different attempts have been made to simulate the long term chemical degradation of concrete [3,4,5,6,7]. In general, four states of cement degradation are identified depending on the pH and cement pore water controlling cement phases (pH-values are for the reference temperature of 25°C). State 1 has a pH larger than 12.5 with a high concentration of Na and K ions. State 2 has a pH of 12.5 controlled by the dissolution of portlandite with approximately

---

[1] *Corresponding author: djacques@sckcen.be

20 mmolal of Ca. State 2 starts when all portlandite has been leached out of the cement and the pH is between 12.5 and 10. The pore water composition is buffered by different cement phases including AFt, AFm and calcium-silicate hydrates (C-S-H phases). The end of this state is defined when all these phases are completely leached out. State 4 has a pH lower than 10 with aggregate minerals present; in this study calcite is the only aggregate used. The pore water composition is then mainly influenced by the composition of the infiltrating water. Although the reactions within each state are quite independent of the composition of the infiltrating water, the duration of the different states and the stoichiometric coefficients of the different dissolution/precipitation reactions depend strongly on the composition of the infiltrating water (see further).

The assessment of the progression of the long-term chemical degradation of cement is possible by means of model simulation. The most straightforward way is using thermodynamic equilibrium modelling coupled with transport of solution species. Such modelling approach is able to reproduce the zoning of cement degradation, as is shown by e.g. Moranville et al. [8]. A more simple approach is to use only thermodynamic equilibrium modelling with a mass balance approach in which, after the equilibrium calculation, the cement-equilibrated pore water is replaced with a new amount of the external aggressive water while keeping the changed cement solid phase. Such type of simulation allows an in-depth analysis of the geochemical changes in both the pore water and the solid phase.

This paper first describes simulations of chemical concrete degradation using thermodynamic equilibrium modelling combined with a mass balance approach for different rain and soil water types accounting for processes as wet deposition, dry deposition, soil biological processes and soil weathering and release of base cations from soils in contact with concrete at ambient surface temperatures (long-term mean temperature of 10°C) using a consistent thermodynamic model for cement phases at temperatures different from the standard temperature (25°C). These calculations were done within the framework of near-surface disposal of low and intermediate-level short-lived radioactive waste in Belgium and coordinated by ONDRAF/NIRAS (Belgian Agency for Radioactive Waste and Enriched Fissile Materials). Atmospheric boundary conditions relevant for determining rain water and soil water composition were taken from nearby meteorological stations. In a second step the mineralogical changes are linked to microstructural changes that determine the pore structure (tortuosity), porosity, hydraulic and transport properties (section 2). A simplified version of this dynamic coupled degradation model is then applied to simulate the degradation of large-scale concrete components of the surface repository (section 3).

1.2. Modelling approach

Chemical degradation of concrete is simulated using mass conservation and thermodynamic equilibrium laws (mass action equations) starting from 1000 cm³ of concrete at a long-term averaged atmospheric temperature (~10°C, representative for Belgium, Jacques and Mallants [9]). The concrete is equilibrated with a given amount of external water (not in equilibrium with the concrete phases). After equilibration, the resulting water is replaced by a new amount of external water whereas the changed cement solid phase is maintained. In this way, the changing cement pore water and solid phase composition is simulated as function of cumulative added (external) water. This approach needs (i) a consistent thermodynamic database for aqueous species and cement phases for 10°C, (ii) the initial concrete composition and (iii) the composition of the external (soil) water types.

1.2.1. Thermodynamic model for cement degradation

A thermodynamic data set for cement minerals was built by Lothenbach and Winnefeld [10], Lothenbach et al. [11] and Matschei et al. [12] consistent with the thermodynamic data in the Nagra/PSI-Thermodynamic Data Base [13]. When used in the geochemical GEMS-software [14], temperature dependences of thermodynamic parameters are calculated with the embedded SUPCRT code [15]. The GEMS-software minimizes the Gibbs free energy of the system subject to a number of constraints (mass balance conditions, electrical neutrality). However, the database is not consistent if it is used at temperatures different from 25°C in geochemical codes as PHREEQC [16] in which geochemical equilibrium is calculated based on mass action equations. To simulate the chemical

degradation due to leaching at a long-term average of the atmospheric temperature (taken to be 10°C in Belgium), the mass action constants of all aqueous species and minerals in the model must be recalculated for this temperature. The Gibbs free energy for all species was calculated with GEMS (based on the revised Helgeson-Kirkham-Flowers equations for aqueous species or the integration of the heat capacity function Cp(T) for minerals and gases) and related to the mass action constant KT by:

$$K_T = \exp\left(-\frac{\Delta_r G_T^\circ}{RT}\right) \tag{1}$$

where R is the universal gas constant, and $\Delta_r G_T^\circ$ is the Gibbs free energy change of a reaction at temperature T:

$$\Delta_r G_T^\circ = -\sum_i v_{ji} \Delta_f G_{T,A_i}^\circ \tag{2}$$

where $\Delta_f G_{T,Ai}^\circ$ is the Gibbs free energy of formation of species A_i at temperature T and v_{ji} are the stoichiometric coefficients of the chemical reaction. A detailed description of the conversion of the GEMS-database to a PHREEQC-database, a list of the aqueous species and minerals in the thermodynamic model and corresponding mass action constants at 10°C are given in Jacques [17][2]. Note that the solubility of Na and K in state 1 were slightly differently treated. Alkali sulphate salts are very soluble resulting in the high Na and K concentrations, but sulphate is buffered by the formation of ettringite. Using the average values of Na and K concentration in ordinary Portland cement as reported by Brouwers and van Eijk [18], solubility of two hypothetical phases (Na_2O and K_2O) were calculated.

TABLE 1 OXIDE AND PHASE COMPOSITION OF CEM I (AFTER [11], ONLY THE FOUR MAJOR CLINKER PHASES ARE GIVEN)

Mineral	g/100 g OPC	Mol / 100 g OPC	Molar mass (g/mol)
CaO	62.4	1.1127	56.0794
SiO_2	18.9	0.3146	60.0843
Al_2O_3	4.4	0.0432	101.961
Fe_2O_3	2.5	0.0157	159.688
CaO(free)	0.6	0.0107	56.0774
MgO	1.4	0.0347	40.3044
K_2O	0.95	0.0101	94.196
Na_2O	0.10	0.0016	61.979
CO_2	2.1	0.0477	44.01
SO_3	3.0	0.0375	80.0652
Alite (C_3S)	58		
Belite (C_2S)	10		
Aluminate (C_3A)	7.6		
Ferrite (C_4AF)	7.5		

---

[2] Available upon request

1.2.2. Concrete composition and initial cement hydrates

Calculations are based on a CEM I 42.5 N composition as given in Lothenbach et al. [11], TABLE 1). The concrete consists of 350 kg CEM I, 1828 kg of different calcareous aggregates and 175 kg water per m³ of concrete (Jacques et al. [19]). Calculated equilibrium concrete pore water composition and mineral phase assemblages are given in TABLE **2**.

TABLE 2 INITIAL PORE WATER COMPOSITION OF 1000 CM³ CONCRETE CONTAINING 350 G CEM I 42.5 N (TABLE 1), 1828 G CALCITE AND 175 G WATER

Element	Concentration (mol/kgw)	Mineral	Amount (mol/1000 cm³ concrete)
Al	1.38E-05	Jen[(1)]	9.95E-01
C	8.25E-05	Tob[(1)]	1.07E-01
Ca	1.58E-03	Ettringite	4.37E-02
K	1.60E-01	Tricarboaluminate	1.36E-02
Mg	1.93E-09	Monocarboaluminate	6.34E-02
Na	6.82E-02	HydrotalciteOH	3.04E-02
S	2.81E-04	Portlandite	1.49
Si	3.40E-5	Na_2O	3.66E-03
pH	13.8	K_2O	3.08E-02
Ionic strength		Calcite (cement)	6.32E-02
	0.22	Calcite (aggregate)	18.26

[(1)] Jen and Tob are the jennite-like and tobermorite-like end members in an ideal solid solution description of the C-S-H phases.

1.2.3. Water composition

The geochemical degradation of concrete depends on the composition of the infiltrated external water beside many other factors. The sensitivity of the chemical degradation rate of concrete for water composition is evaluated by doing several simulations with different water types. Water compositions used in the simulations are given in TABLE 3.

TABLE 3 OVERVIEW OF THE COMPOSITION OF THE INFILTRATED WATER. TYPE 1 AND 2 ARE RAIN WATER TYPES FOR WET DEPOSITION ONLY (TYPE 1) AND FOR WET AND DRY DEPOSITION (TYPE 2) WITH ATMOSPHERIC PARTIAL PRESSURE OF $CO_2(G)$ (= $10^{-3.5}$ ATM). TYPE 3 IS THE WET AND DRY DEPOSITION CASE WITH SOIL PARTIAL PRESSURES OF $CO_2(G)$ (= $10^{-2.3}$ ATM). TYPE 4 AND 5 ARE SOIL WATER TYPES WITH SOIL WEATHERING AND AL IN EQUILIBRIUM WITH GIBBSITE (TYPE 4) OR DERIVED FROM WEATHERING RATES (TYPE 5)

Water type	1 Rain water – wet only	2 Rain –water – bulk deposition	3 Soil water – CO_2	4 Soil water – gibbsite	5 Soil water – weathering
Al	-	-	-	$1.02\ 10^{-5}$	$4.48\ 10^{-5}$
C	$1.70\ 10^{-5}$	$1.70\ 10^{-5}$	$2.67\ 10^{-4}$	$2.72\ 10^{-4}$	$2.70\ 10^{-4}$
Ca	$5.00\ 10^{-6}$	$5.35\ 10^{-5}$	$5.35\ 10^{-5}$	$5.71\ 10^{-5}$	$5.71\ 10^{-5}$
Cl	$5.12\ 10^{-5}$	$1.82\ 10^{-4}$	$1.82\ 10^{-4}$	$1.82\ 10^{-4}$	$1.82\ 10^{-4}$
K	$3.80\ 10^{-6}$	$2.94\ 10^{-5}$	$2.94\ 10^{-5}$	$6.53\ 10^{-5}$	$6.53\ 10^{-5}$
Mg	$5.00\ 10^{-6}$	$2.27\ 10^{-5}$	$2.27\ 10^{-5}$	$2.53\ 10^{-5}$	$2.53\ 10^{-5}$
N(5)	$1.17\ 10^{-4}$	$4.12\ 10^{-4}$	$4.12\ 10^{-4}$	$3.54\ 10^{-4}$	$3.54\ 10^{-4}$
Na	$4.40\ 10^{-5}$	$1.79\ 10^{-4}$	$1.79\ 10^{-4}$	$2.05\ 10^{-4}$	$2.05\ 10^{-4}$
S	$3.50\ 10^{-5}$	$1.19\ 10^{-4}$	$1.19\ 10^{-4}$	$1.19\ 10^{-4}$	$1.19\ 10^{-4}$
					-
pH	3.78	3.34	3.34	4.41	3.73
IS^1	$2.82\ 10^{-4}$	$1.02\ 10^{-3}$	$1.02\ 10^{-3}$	$1.18\ 10^{-3}$	$1.07\ 10^{-3}$

The first two types of water are so-called rain water types. Type 1 is defined by assuming that the water infiltrating the concrete has the same composition as the rain water. This type is indicated as Rain water – "wet only deposition" and representative values were obtained from a series of averaged yearly concentrations as measured in the Dutch 'National Precipitation Chemistry Network' (as cited in Jacques et al. [19]). The only biological process taken into account for this type of water is total nitrification of the ammonium. Another rain water variant (type 2) takes into account the bulk dry deposition in calculating its chemical composition. In this study, this so-called "Rain water – bulk deposition" is represented by long term (1993-2002) annual averaged bulk deposition amounts measured at the open field as reported in Neirynck et al. [20]. Deposition values reported as keq/ha/year are converted to mol/kg water using the average annual precipitation surplus (= precipitation – actual evapotranspiration, [19]).

A second group of water types are those in which the rain water, prior to contacting the concrete, is flowing through soil layers resulting in composition changes due to (micro)biological respiration and soil weathering processes. Soil microbiological respiration increases the partial pressure of $CO_{2(g)}$ in the soil gas phase compared to the partial pressure of $CO_{2(g)}$ of the atmosphere. The increase in partial pressure depends on the availability of energy and water in the plant-soil environment. The model of Brook et al. [21] for predicting the partial pressure of $CO_{2(g)}$ in the soil gas phase uses the yearly actual evapotranspiration as a surrogate for both available water and energy:

$$\log(P_{CO2}) = -3.47 + 2.09\left(1 - e^{-0.00172ET_a}\right)$$

$$(3)$$

where P_{CO2} is the partial pressure of $CO_{2(g)}$ in the soil gas phase (atm) and ET_a is the annual actual evapotranspiration (mm). The latter was calculated for typical weather conditions in North-Belgium using a 37-year long climatological record for a sandy soil covered with grass (for details, see [9]). Also the second typical soil process (weathering) is estimated in a generic way using only a limited amount of information on soil texture and parent material class used to define a weathering rate class [22]. The yearly weathering rate of base cations (Na, K, Ca, Mg) is calculated as:

$$BC_w = z\,500(WRc - 0.5)\exp\left(\frac{A}{281} - \frac{A}{273 + T}\right) \qquad (4)$$

where BC_w is the weathering rate of base cations (eq/ha/yr), T is the average yearly soil temperature (10°C), WRc is the weathering rate class (1 for a sandy soil), z is the soil depth (1 m) and $A = 2\,600$ K. The fractions of the individual cations were based on the average total cation contents for acid sandy soils reported in De Vries [23] and are fixed at 0.35, 0.49, 0.10 and 0.07 for Na, K, Ca and Mg, respectively.

Three types of soil water were defined: (i) only accounting for soil biological respiration processes ("Soil water – CO_2", type 3) (ii) accounting for soil biological respiration processes and base cation weathering, in which the Al concentration is calculated in equilibrium with the soil mineral gibbsite ("Soil water – gibbsite", type 4), and (iii) the same as "Soil water – gibbsite", but the Al concentration is obtained from multiplying the base cation weathering rate with a factor of 2 [22] ("Soil water – weathering", type 5).

Some general assumptions were made in the derivation of the soil water type with respect to the very long time scale considered in chemical degradation of concrete. Basically, assumptions were made to apply a static mass-balance approach for calculating the soil influence on the composition of the infiltrating water. For example, ion exchange and sorption processes in the soil are not taken into account because they are considered as finite buffering processes. On the long term, the soil exchange complex is in equilibrium with the soil water composition. Other assumptions are listed in [19].

1.3. Results and discussions

1.3.1. *Cement degradation during leaching with rain water*

FIG. *1* shows some simulation results for the "Rain water – wet deposition only". The four major states of geochemical concrete degradation are indicated by colour bands. State 1 is characterized by high Na and K concentrations (simulated here in equilibrium with the surrogate alkali oxides, Na_2O and K_2O). The resulting pH is very high: 13.8 at 10°C. The concentration of the elements is not controlled by the composition of the infiltrating water, but by the dissolution of the cement phases. This results in large changes in concentrations: a five orders of magnitude increase in concentrations of Na and K, a three-orders of magnitude decrease and increase in Mg and Ca concentrations, respectively, and about one order of magnitude increase of sulphate concentration. The first state ends after approximately 0.35 kg of added water per 1 000 cm³ concrete.

The second state is characterized by portlandite dissolution with a pH of 13.05 at 10°C (at 25°C, it is about 12.5). Concentrations of all elements are still controlled by the cement phases, except Na and K concentrations that are still governed by the rain water. This state ends after approximately 72 kg of added water per 1 000 cm³ concrete. The dissolution of portlandite resulted in an increase in porosity of about 4.9%.
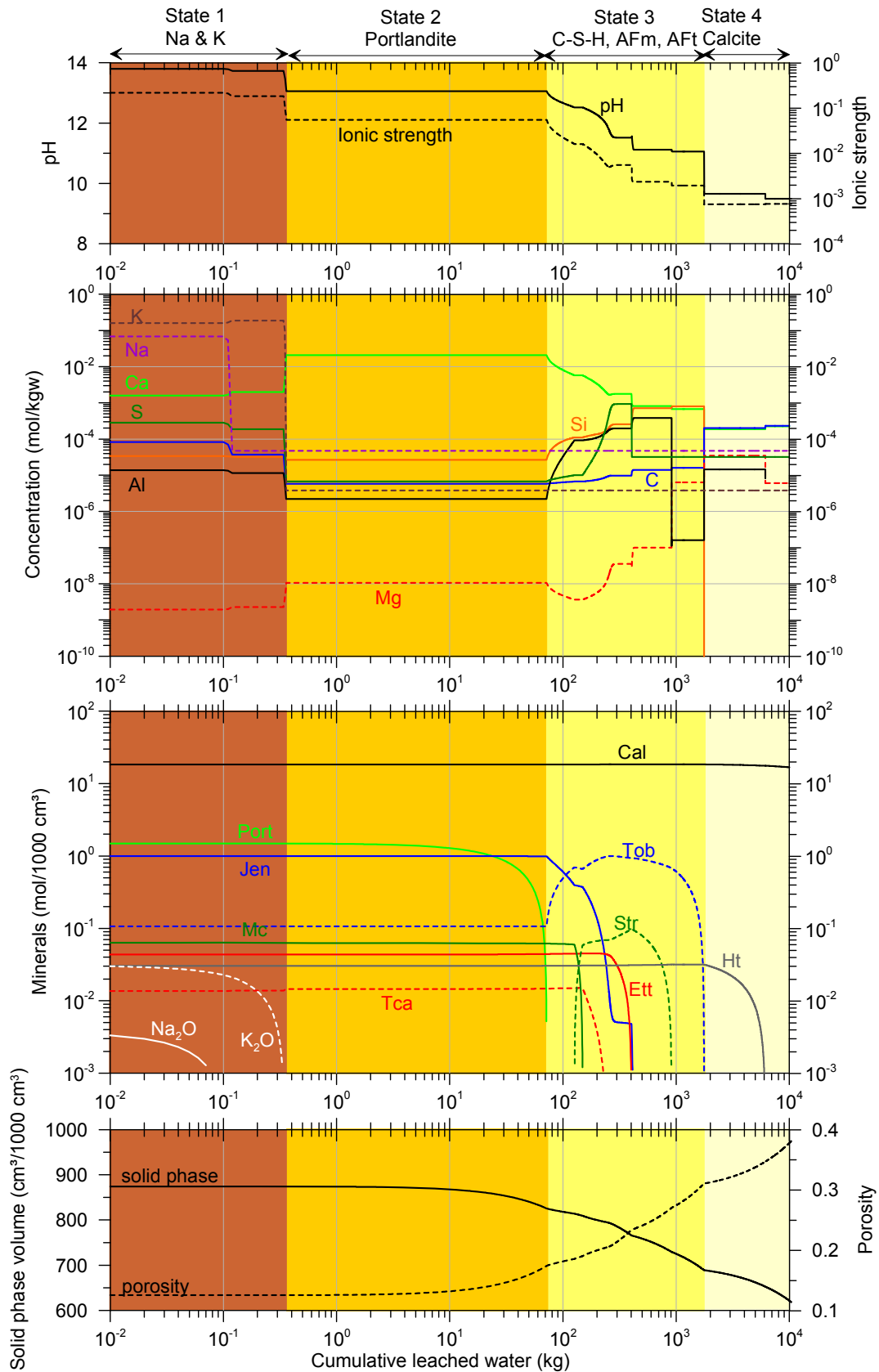
FIG. 1 Geochemical changes during leaching of 1 000 cm³ concrete with Rain water – wet deposition only (type 1) at 10°C. Port: Portlandite, Jen: Jennite-like end member, Tob: Tobemorite-like end member, Mc: Monocarboaluminate, Ca: Calcite, Str: Strätlingite, Tca: Tricarboaluminate, Ett: Ettringite, Ht: OH-hydrotalcite. Colours panes refer to consecutive concrete degradation States I to IV.

The third state is geochemically the most complex state with a sequence of mineral dissolution and precipitation reactions with changing dissolution and precipitation reactions of the C-S-H, AFm and AFt phases. Its end is defined by the complete dissolution of the C-S-H tobermorite-like end member. Within this state, the solution composition drastically changes with a decrease in pH to 11.06 and up to one order of magnitude changes in solute concentrations. Following sequence of cement phase dissolution and precipitation reactions is identified:

— Reaction 1: Decalcification of the C-S-H phase by partly transformation of the jennite-like end member to the tobermorite-like end member resulting in a decreasing Ca / Si ratio of the solid phase,

— Reaction 2: Complete dissolution of monocarboaluminate with co-dissolution of the C-S-H phase and precipitation of strätlingite and calcite,

— Reaction 3: Complete dissolution of tricarboaluminate with co-dissolution of the jennite-like end member of the C-S-H phase and precipitation of calcite and the tobermorite-like end member of the C-S-H phase,

— Reaction 4: Complete dissolution of ettringite with co-dissolution of the tobermorite-like end member of the C-S-H phase and precipitation of strätlingite,

— Reaction 5: Complete dissolution of the jennite-like end member of the C-S-H phase together with co-dissolution of the tobermorite-like end member and strätlingite,

— Reaction 6: Complete dissolution of strätlingite with co-dissolution of the tobermorite-like end member in the C-S-H phase,

— Reaction 7: Complete dissolution of the tobermorite-like end member in the C-S-H phase.

These main dissolution and precipitation reactions go together with some minor equilibrium reactions controlling the cement pore water composition. Sulphate and silicium concentrations are equal to the concentrations in the rain water ([Si] = 0 M) after, respectively, the complete dissolution of ettringite and the tobermorite-like end member in C-S-H. During this state, silicium concentrations increase but the concentrations never exceeded the solubility of amorphous silicium dioxide. This state ends after approximately 1 766 kg of water added per 1000 cm³ concrete. Due to the dissolution of the voluminous AFt and AFm phase, the porosity also increases significantly in state 3.

In state 4, OH-hydrotalcite and calcite (both from the cement phase and from the calcareous aggregates) are present. OH-hydrotalcite first dissolves completely with co-dissolution of calcite needing approximately 4 400 kg of water per 1 000 cm³ concrete, followed by a slow dissolution of calcite dissolving 2.2×10^{-4} mol calcite per kg of water added.

The same sequence of states and reactions in state 3 were simulated for the "Rain water – bulk deposition" case (FIG. *2*a – only the solid phase composition is shown). However, this rain water composition results in a faster chemical degradation of concrete compared to "Rain water – wet deposition only". State 3 needs 246 kg of water per 1 000 cm³ less than the "Rain water – bulk deposition". A different reaction sequence is simulated for state 4: OH-hydrotalcite is first converted in CO_3-hydrotalcite with precipitation of $Al(OH)_3$ due to the lower pH of the soil water composition. When all OH-hydrotalcite is dissolved, the CO_3-hydrotalcite is dissolving together with calcite and precipitation of $Al(OH)_3$ occurs. After 2 606 kg of water is added per 1 000 cm³ concrete, only calcite and $Al(OH)_3$ are dissolving.
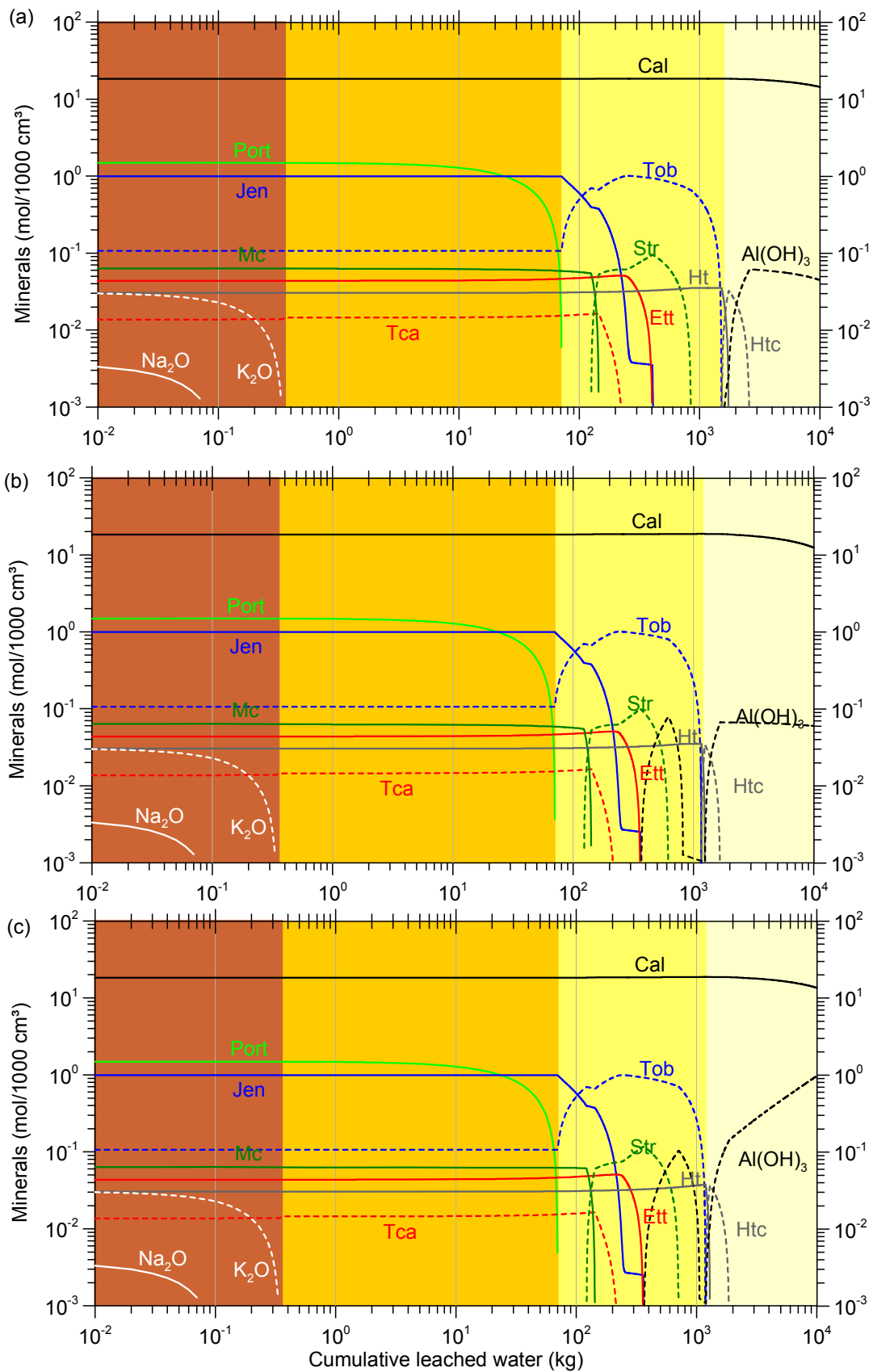
FIG. 2 Geochemical changes during leaching of 1000 cm³ concrete with (a) Rain water – bulk deposition (type 2), (b) Soil water – CO₂ (type 3), and (c) Soil water – gibbsite (type 4) at 10°C. Port: Portlandite, Jen: Jennite-like end member, Tob: Tobemorite-like end member, Mc: Monocarboaluminate, Ca: Calcite, Str: Strätlingite, Tca: Tricarboaluminate, Ett: Ettringite, Ht: OH-hydrotalcite, Htc: CO₃-hydrotalcite. Colours panes refer to consecutive concrete degradation States I to IV.

1.3.2. Cement degradation during leaching with soil water

A first calculation case with soil water is the one where biological processes were taken into account by increasing the partial pressure of $CO_2(g)$ in the soil gas phase to $10^{-2.3}$ atm (based on Eq. (3)). Mineralogical changes are shown in FIG. $\textbf{2}$b. A large difference with the rain water cases is the precipitation of calcite in all degradation reactions during states 1, 2, and 3, whereas calcite was only formed during the dissolution of the carbonate-bearing minerals (monocarboaluminate and tricarboaluminate) in the cement matrix for the rain water types. The calcite is formed here by the process of carbonation in which dissolved inorganic carbon present as CO_3^{2-} at the high pH conditions is available to react with free calcium ions (Ca^{2+}). Calcite is shown to be the main product of carbonation and not its polymorphs aragonite and valerite [2]. The free Ca^{2+} ion originates from the dissolution of the Ca-bearing cement phases. During state 1 and 2, portlandite is the main source for the calcium ion. Due to this carbonation, the amount of water needed to end state 3 is less compared to the rain water types: 1162 kg of water per 1 000 cm³ concrete compared to 1 520 kg of water for the rain water (type 2). Note also that during the dissolution reaction of strätlingite and the tobermorite-like end member in the C-S-H phase (reaction nr 6), $Al(OH)_3$ precipitation is simulated which then subsequently dissolves completely during dissolution of the tobermorite-like end member.

The last two simulations are those accounting also for weathering of the soil mineral phases. The main difference with the previous calculations is the presence of aluminium in the water by assuming equilibrium with gibbsite (Soil water – gibbsite) or deduced from the base cation weathering rate (Soil water – weathering). The two simulations are very similar thus only "Soil water – gibbsite" is shown in FIG. $\textbf{2}$c. The sequence of reactions in state 1 to 3 is identical to the previous simulation (Soil water – CO_2) with a slightly larger amount of water needed to end state 3. During state 4, first OH-hydrotalcite is transformed to CO_3-hydrotalcite. The latter dissolves then, followed by the dissolution of calcite. Contrary to the case "Soil water – CO_2", $Al(OH)_3$ is still precipitating. This results in a slightly smaller increase in porosity during state 4 compared to the "Soil water – CO_2" case.

1.3.3. Comparison of simulation cases

TABLE 4 gives the cumulative amount of water needed per 1 000 cm³ concrete to end states 1, 2 and 3. The end of states 1 and 2 is relatively insensitive to the composition of the infiltrating water, except that the "soil water" types are slightly more aggressive. The difference between the fastest and slowest end of state 3 is about 540 kg of water per 1 000 cm³ concrete.

TABLE 4 OVERVIEW OF THE AMOUNT OF WATER NEEDED (KG) TO END THE FIRST THREE STAGES FOR 1000 CM³ OF CONCRETE (STATE 4 NEVER ENDED BEFORE THE SIMULATED 10000 KG OF CUMULATIVE LEACHED WATER)

	Type 1	Type 2	Type 3	Type 4	Type 5
State 1	0.35	0.35	0.35	0.35	0.35
State 2	72	72	71	70	70
State 3	1766	1520	1162	1185	1203

The "Rain water – bulk deposition" water type is more aggressive compared to the "Rain water – wet only" water type. Whereas the composition of the wet deposition is in general more predictable from factors as distance from the sea and main wind direction, the bulk deposition prediction is much more difficult because it depends on surface characteristics, vegetation type, local-scale wind direction, industrial activities in the surroundings (Appelo and Postma [24]). For example, forests change significantly the composition of the throughfall water by different crown exchange processes. Hansen and Postma [25] showed that concentrations in aquifers may vary up to a factor 10 depending on the location of the measurement location (near the windward margin of a forest, or inside the forest). In

that sense, the impact of dry deposition on the long-term durability of concrete used e.g. in near-surface disposal facilities is relatively uncertain.

Increasing the partial pressure of $CO_{2(g)}$ from atmospheric conditions ($P_{CO2} = 10^{-3.5}$ atm) to soil conditions accounting for biological activity ($P_{CO2} = 10^{-2.3}$ atm) reduced the water needed to end state 3 by about 350 kg of water per 1 000 cm³ concrete. Putting a soil cover on top of a concrete-based repository may thus have negative effects on the long-term chemical durability due to an increased carbonation with inorganic carbon originating from biological processes. However, a soil layer also has positive effects on durability, i.e. it (i) protects the concrete from physical degradation processes such as raindrop impact erosion and abrasive erosion when exposed directly to atmospheric conditions, (ii) buffers freezing and thawing cycles, (iii) limits the impact of biological agents (roots, organic acids) and (iv) reduces water percolation by evapotranspiration processes.

The weathering process simulated here using a generic base cation weathering rate, has a small but beneficial effect on the chemical durability of the concrete. For the relative inert sandy soil material considered in this study, the end of state 3 is only delayed for about 20 to 40 kg of water per 1 000 cm³ concrete. However, when heavy clay is used to cover the concrete, the base cation weathering rate is significantly higher resulting in higher base cation concentrations, higher Al and Si concentrations and a higher pH. This all results in a longer durability of the concrete [19].

The variability in the soil solution composition is illustrated by comparing the simulated Ca concentrations for the different water types in FIG. *3*a. The composition of the infiltrating soil water is only of minor importance in state 1, 2 and a part of state 3. The cement pore water is then mainly buffered by the cement phases. After tricarboaluminate is dissolved, variation between the cases increases, partly because the influence of the composition of the percolation water becomes more important during the leaching process. Another factor is that, once a certain amount of cumulative water has been added, there is a larger variation in the specific dissolution reactions between the different water types because the stability of the cement depends on the aggressiveness of the percolating water. A similar behaviour is simulated for the other elements with the exception of elements controlled by the concentration in the incoming water when the cement hydrates controlling these elements are depleted (e.g., Na en K).

FIG. *3*b shows the weight percentage of the C-S-H phase as function of the cumulative amount of water per 1 000 cm³ concrete. This is of particular interest because the C-S-H phase plays an important role in the sorption and retardation of contaminants [1]. As was observed for Ca, the decrease is quite similar between the different cases as long as monocarboaluminate and tricarboaluminate are present. When these two cement phases are completely dissolved and leached out, variation between the different water types increases [33].
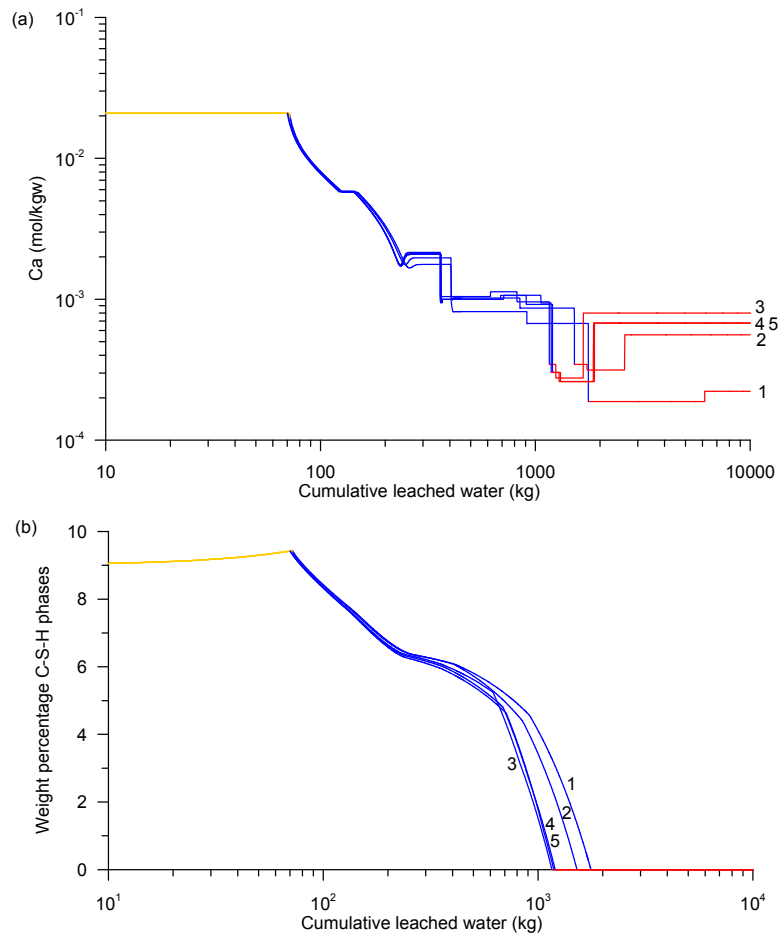
FIG. 3 (a) Ca evolution and (b) C-S-H weight percentage evolution as a function of cumulative leached water in 1000 cm³ concrete for 5 different water compositions. The four states are indicated by colours: state 2 is yellow, state 3 is blue and state 4 is red. Numbers refer to the water types as defined in Table 3.

1.4. Conclusions

This chapter described the chemical degradation of concrete as a function of cumulative percolated amount of water for different water types. The sequence of mineralogical changes in the cement is relatively insensitive with respective to the water type composition. The overall description of four chemical degradation states of concrete during leaching is encountered in the simulations, with state 3 encompassing the dissolution of AFm, AFt and C-S-H phases the chemically most complex state. These cement phases do not dissolve in a successive sequence, but in a complex way, e.g. transforming first the AFm phase monocarboaluminate in strätlingite, followed by ettringite dissolution and followed by strätlingite dissolution.

In contrast to the sequence of mineralogical changes, the duration of the different states and dissolution reactions – as measured by the cumulative amount of water needed to end a state or dissolve completely a given cement phase – depends strongly on the external water composition: the more aggressive external water is, the faster the cement degradation proceeds. In that respect, dry deposition of various chemicals contributes significantly to the aggressiveness of the percolating water. Unfortunately, this contribution of dry deposition to rain chemical composition water is relatively unpredictable for long term assessments because it depends on many local-scale surface factors such as vegetation and industries. Biological soil processes are also an important factor in increasing the water aggressiveness by increasing the inorganic carbon content in the percolating water (higher carbonation rate). This increase was predicted here by an empirical model relating the annual partial pressure of $CO_{2(g)}$ in the soil air phase to actual evapotranspiration, a surrogate for

available energy and soil moisture. Weathering of soil minerals decreases again the aggressiveness of the percolating water. In this study, the positive effect of the soil layer on decreasing aggressiveness of water was minimal because relatively inert sandy material was taken.

2. REACTIVE TRANSPORT MODELLING OF CHEMICAL DEGRADATION OF CEMENT-BASED SYSTEMS: DYNAMIC TRANSPORT PROPERTIES COUPLED WITH GEOCHEMICAL EVOLUTION

2.1. Introduction

Concrete engineered systems will undergo chemical changes due to interaction with the potentially damaging surroundings. Typical chemical detrimental reactions of concrete are chloride ingress, carbonation, decalcification and sulphate attack [26]. One of the most typical reactions is the dissolution or precipitation of cement hydrates and minerals. This, in turn, can change the porosity of the concrete which also affects processes and properties related to water flow, heat transport and solute transport. Numerical tools integrating conceptual models for all these processes allow the assessment of degradation fronts due to chemical detrimental processes in concrete systems. Some examples of modelling these coupled processes in concrete systems were given by Pfingsten et al. [27], Moranville et al. [8], Galindez et al. [28], and van der Lee et al. [29], amongst others. The objective of this study is to simulate the long term chemical degradation of concrete taking into account the feedback of geochemical reactions on porosity and porosity-related hydraulic and transport properties with the reactive transport code HP1 [30, 31, 32][3].

2.2. Thermodynamic modelling of cement systems

Lothenbach et al. [11] defined a thermodynamic database for cement hydrates consistent with the thermodynamic data in the NAGRA/PSI-Thermodynamic Database [13]. Jacques [17] converted the CEMDATA07 database to a database in PHREEQC-format (code based on solving a system of mass action equations). The database implements mass action constants for C-S-H phases which are modelled as an ideal solid solution between jennite and tobermorite, AFt phases with a non-ideal solid solution between ettringite and tricarboaluminate, hydrogarnet, AFm phases represented by a series of hydrates such as C_2AH, C_4AH_{13}, monosulfoaluminate, monocarboaluminate, hemicarboaluminate, and strätlingite, and hydrotalcite and a carbonate form of hydrotalcite (CO_3-hydrotalcite).

Jacques et al. [33] used the complete CEMDATA07 thermodynamic database to model cement degradation by different water types in terms of cumulative amount of input water (see higher). To overcome problems with numerical convergence when porosity and porosity-related hydraulic and transport properties are updated every time step, only a subset of cement minerals was selected from the database for transport simulations in this study. Only the cement hydrates formed in these simulations are retained in the reactive transport example discussed below. In addition, the non-ideal solid solution between ettringite and tricarboaluminate is replaced by an ideal solid solution. The geochemical model thus includes the following cement hydrates: portlandite (Port), monocarboaluminate (Mc), strätlingite (Strat), calcite (Cal), OH-hydrotalcite (Ht), CO_3-hydrotalcite (Htc), the ideal solid solution between jennite (Jen) and tobermorite (Tob), and the ideal solid solution between ettringite (Ett) and tricarboaluminate (Tca).

2.3. Flow and transport in variably-saturated concrete

Water flow in variably-saturated concrete at the continuum scale is described by a combination of mass conservation and the Darcy-Buckingham relation, which results in the Richards equation. The one-dimensional form of it is written as (Mallants et al. [34]):

---

[3] Avaialable at: http://www.pc-progress.com/en/Default.aspx?h1d-hp1

$$\frac{\partial \theta}{\partial t} = \frac{\partial}{\partial x}\left[K_s K_r(h)\left(\frac{\partial h}{\partial x} + \cos\gamma\right)\right] \tag{5}$$

where h is the pressure head [L], θ is the water content [$L^3 L^{-3}$], t is time [T], x is the spatial coordinate [L], γ is the angle between the flow direction and the vertical axis, K_s is the saturated hydraulic conductivity [$L\ T^{-1}$] and K_r is the relative hydraulic conductivity [-]. Transport of the aqueous components is described by the advection-dispersion equation which is written for one-dimensional system as (Mallants et al. [34]):

$$\frac{\partial \theta C_j}{\partial t} = \frac{\partial}{\partial x}\left[\theta D\left(\frac{\partial C_j}{\partial x}\right)\right] - \frac{\partial q C_j}{\partial x} + R_j \tag{6}$$

where C_j is the total dissolved concentration of the jth component [$M\ L^3$], D is the hydrodynamic dispersion coefficient [$L^2\ T^{-1}$], q is the volumetric fluid flux density [$L\ T^{-1}$] and R_j is the source / sink term of the jth component due to geochemical reactions [$M\ L^{-3}\ T^{-1}$]. The hydrodynamic dispersion coefficient is obtained by (Mallants et al. [34]):

$$\theta D = \theta D_w \tau_w + \lambda q \tag{7}$$

where D_w is the diffusion coefficient in pure water [$L^2\ T^{-1}$], τ_w is the tortousity factor in the liquid phase [-], and λ is the dispersivity [L]. The tortuosity factor is a material property but depends also on the porosity of the porous medium.

In case R_j contains solid phase precipitation and dissolution reactions, the porosity changes with time. This also affects other transport-related parameters such as the permeability k or the tortuosity. A straight-forward way to account for these geochemically-induced changes in transport parameters at a continuum scale is by defining relationships between the macroscopic variable porosity and the other transport parameters. Kozeny-Carman type of equations is frequently used to relate the permeability to the porosity. Recently, Wissmeier and Barry [35] developed a relation based on the selective radius shift and the continuous film model for saturated flow conditions:

$$a_K = \frac{K_s}{K_{s0}} = \frac{k}{k_0} = \left(\frac{\varphi}{\varphi_0}\right)^l \left(\frac{\varphi - \theta_r}{\varphi_0 - \theta_r}\right)^{8/3} \tag{8}$$

where a_K is the scaling factor for the conductivity, K_{s0} and k_0 are the initial saturated hydraulic conductivity and the permeability, respectively, l is the pore connectivity factor [-], and θ_r is the residual water content. Based on microstructural modelling, Garboczi and Bentz [36] derived a relationship between porosity and tortuosity for cementitious systems:

$$\tau_w = 0.001 + 0.07\varphi + 1.8H(\varphi - \varphi_c)(\varphi - \varphi_c)^2 \tag{9}$$

where H() is the Heavyside function and φ_c is the critical capillarity porosity of the material.

2.4. Example of reactive transport modelling with feedback to tortuosity, porosity, and permeability

2.4.1. HP1 numerical code

HP1 is a simulator for reactive transport modelling in variably-saturated porous media [31]. The coupled solute transport and geochemical equations are solved by a sequential non-iterative algorithm by coupling two existing codes: HYDRUS-1D [37] to simulate water flow, heat transport and multi-component solute transport and PHREEQC [16] to simulate thermodynamic and kinetic

biogeochemical processes. Version 2.2.002 of HP4 [38] was used as the basis to include porosity, permeability and tortuosity changes induced by geochemical reactions and processes. The specific relations between geochemical state variables (amount of the different reactive solid phases), porosity, permeability and tortuosity are hard-coded in HP1. Rather users have a large flexibility to define their own relations through the BASIC-interpreter incorporated in PHREEQC. The example discussed below uses the formulations as defined in Eqs. (8) and (9).

2.4.2. *Example of leaching/decalcification*

Leaching/decalcification of an Ordinary Portland Cement (OPC) – cement based concrete is used as an illustration. The concrete is based on CEM I (350 kg CEM I) mixed with 1828 kg of different calcareous aggregates (assumed to be inert) and 175 kg water per m³ concrete. The composition of the OPC cement (as used in the simulation) is 62.4 g CaO, 18.9 g SiO_2, 4.4 Al_2O_3, 1.4 g MgO, 2.1 g CO_2, and 3.0 g SO_3 per 100 g OPC. Simulations are done for a 10-cm long concrete sample with following initial physical properties: $\theta = 0.126$, $K_s = 4.58 \times 10^{-11}$ m/s and $\lambda = 0.001$ m. The pure water diffusion coefficient D_w is 2.3 x 10^{-9} m²/s for all dissolved species. A constant pressure head condition ($h = 0$ cm) is applied at the top boundary. The upper solute transport boundary condition is a constant concentration flux boundary condition with following composition (representative for rain water [33]): [C] = $1.1 \times$x10^{-5} M, [Ca] = 5.5×10^{-6} M, [Cl] = 5.2×10^{-5}, [K] = 3.8×10^{-6}, [Mg] = 6.0×10^{-6} M, [Na] = 4.7×10^{-5} M, [NO_3] = 1.2×10^{-4} M, and [S] = 3.2×10^{-5} M with a pH of 3.8 at 25 ºC. The focus of the discussion is on the transient physical properties of the concrete system. The reader is referred to Jacques et al. [33] for an in depth discussion on the geochemical evolution of the system (although without any feedback to the physical evolution). Note that mechanical processes and their effect on the physical properties are not yet accounted for in these simulations.

---

[4] HP1 is embedded in the HYDRUS-1D software package and is freely available at www.pc-progress.cz.
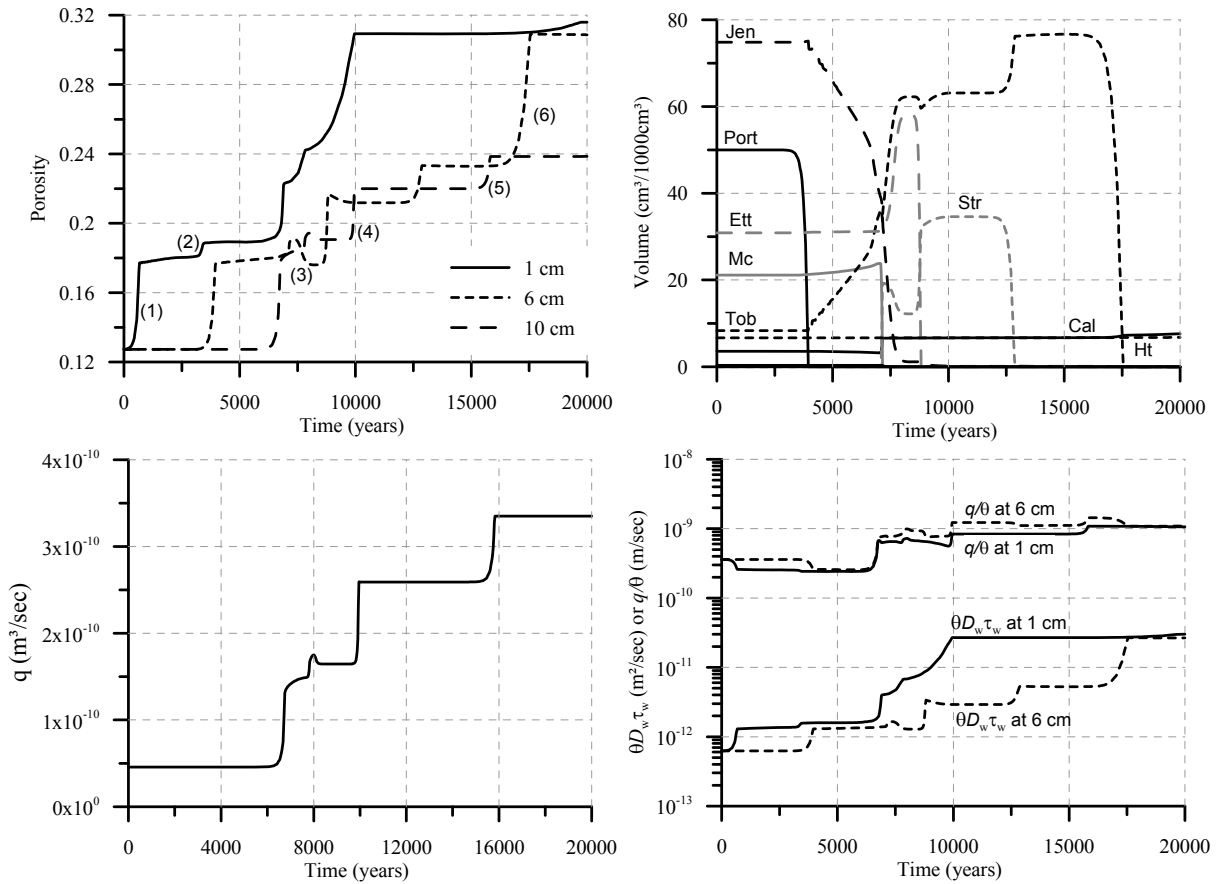
FIG. 4 (a) Time series of porosity for selected depths, (b) time series of volume of the cement minerals at a depth of 6 cm, (c) time series of water flux through concrete column, and (d) time series of θ D_wτ_w and q/ θ at two depths. Numbers in plot (a) are explained in the text; abbreviations in plot (b) are defined in section 2.

FIG. **4** summarizes selected output for a calculation period of 20 000 y. FIG. **4**a shows the porosity at several depths. The significant changes in porosity coincide with main mineralogical changes (FIG. **4**b shows the volumes of the different cement phases as a function of time at a depth of 6 cm): (1) portlandite dissolution, (2) monocarboaluminate dissolution, (3) ettringite precipitation which results in a porosity decrease at the larger depths, (4) ettringite dissolution, (5) strätlingite dissolution, and (6) tobermorite dissolution. Over a period of 20 000 y, porosity increases with a factor of about 2.5. The scaling factor of the conductivity increases from about 3 after complete portlandite dissolution up to about 16 after complete tobermorite dissolution at a given depth. The increase of the tortuosity is also a factor of about 20. However, the increase in water flux through the concrete system occurs only when the porosity has increased throughout the complete column (FIG. **4**c). For example, water flux remains at its initial value for about 6 000 y. Only when portlandite begins to dissolve in the deepest depth (10 cm), the water flux also increases. A series of vertically variable hydraulic conductivities acts as electrical resistors in series; the smallest values determine the flux through the entire system and, thus, the effective hydraulic conductivity (i.e. at the scale of interest which is a 10-cm long column here). Consequently, the local (i.e., point value at specific depth) average solute transport velocity (q/θ) varies also in a step-wise manner although the local porosity has also a small influence (FIG. **4**b). On the other hand, the effective diffusion coefficient ($\theta\ D_w\tau_w$) shows a large spatial variability because it depends on both the local porosity and the local tortuosity factor (FIG. **4**b).

16

2.5. Conclusion

This study combines the implementation of a general formalism of relations between porosity and hydraulic conductivity or tortuosity with the reactive transport code HP1 for variably-saturated porous media by the definition of a scaling factor for the hydraulic conductivity and the tortuosity factor. An important aspect is that these formalisms are hard code in the source code of HP1, but that users can implement different relations defined in the literature. In addition, the user has also significant freedom in defining the chemical system. This study included a state-of-the-art thermodynamic model for cement phases in a transport simulation of chemical degradation of concrete induced by intrusion of rain water. The model was able to successfully demonstrate the impact on the transport properties, i.e. increase with time for the chosen problem, as a consequence of geochemical perturbations. Further work will concentrate on the sensitivity of the degradation rate with respect to different relations between porosity and the transport properties and to the different parameters in these relations.

3. APPLICATION OF A COUPLED DEGRADATION MODEL TO LARGE-SCALE CONCRETE STRUCTURES: MODELLING OF LONG-TERM CHEMICAL DEGRADATION OF FRACTURED CONCRETE STRUCTURE

3.1. Implementation of abstracted model into continuum model

The thermodynamic cement model discussed in section **Error! Reference source not found.** is far too complex to be used in a dynamic simulation of cement leaching at the scale of a real facility. The cement model therefore has to be simplified or abstracted into a form that can be integrated in the convection-dispersion equation for calculating leaching of major elements that determine the cement evolution. The mathematical equations developed here were implemented in the generic simulator COMSOL Multiphysics [39].

An abstracted model of concrete degradation is derived in the form of a calcium-based leaching model. The calcium leaching process is based on the thermodynamic modelling, described in detail in section. As shown in the previous chapter, all variable physical quantities depend on the solid calcium concentration. This is explained by the fact that the dissolved calcium in the porewater exhibits solubility limitation, causing the concentration in the liquid phase to remain constant according to the solubility limit. This property, in turn, disables the use of evolving physical properties based on liquid phase Ca concentrations, as the latter remains constant while solubility limited, although the solid phase (i.e. hardened cement) is loosing material. As an alternative, the solid calcium concentration is used instead.

The approach uses a mass balance of Ca^{2+} ions in the pore fluid, while the dissolution of Portlantide and decalcification of C-S-H are calculated on the basis of the chemical equilibrium between the calcium concentration in the solution and the main solid phases:

$$\frac{\partial(\theta \cdot c_{Ca,aq})}{\partial t} = \nabla \cdot \left(\theta \cdot D_p \nabla c_{Ca,aq}\right) - \frac{\partial c_{Ca,s}}{\partial t}, \tag{10}$$

where $c_{Ca,aq}$, θ, D_p and $c_{Ca,s}$ are calcium concentration in the liquid phase, porosity, pore water diffusion and calcium concentration in the solid phase, respectively. The last term in equation (10) depends on the calcium concentration in solution and is as such strongly non-linear because a non-linear isotherm was invoked to describe the relationship between liquid and solid phase Ca. This is a simplification, as it assumes that sorption is constantly occurring at an equilibrium, thus neglecting the any kinetics. Hence, the relation between solid and liquid phase calcium is expressed in terms of a linear sorption K_d as given in equation (11).

$$K_d = \frac{\partial c_{Ca,s}}{\partial c_{Ca,aq}} \tag{11}$$

Equation (10) can be written more generally, including the solid part as

$$\frac{\partial(\theta(c_{Ca,s}) \cdot c_{Ca,aq})}{\partial t} + \frac{\partial(\rho_b(c_{Ca,s}) \cdot K_d(c_{Ca,s}) \cdot c_{Ca,aq})}{\partial t} = \nabla \cdot \left(\theta(c_{Ca,s}) \cdot \xi(c_{Ca,s}) \cdot D_p \nabla c_{Ca,aq} \right), \tag{12}$$

where bulk density ρ_b and tortuosity ξ are additional physical parameter dependent on the solid calcium concentration. Implementation of equation (11) into equation (12) gives the following partial differential equation expressed in terms of the solid phase Ca:

$$\frac{\partial}{\partial t} \left(\theta(c_{Ca,s}) \cdot \frac{c_{Ca,s}}{K_d(c_{Ca,s})} + \rho_b(c_{Ca,s}) \cdot c_{Ca,s} \right) = \nabla \cdot \left(\theta(c_{Ca,s}) \cdot \xi(c_{Ca,s}) \cdot D_p \nabla \frac{c_{Ca,s}}{K_d(c_{Ca,s})} \right). \tag{13}$$

The drawback of the solid calcium concentration formulation is the discontinuity of temporal and spatial derivatives originating from the relation $c_{Ca,s}/K_d(c_{Ca,s})$.

A mathematically more elegant way to use liquid calcium concentration is to "tailor" the infinite K_d at both high and low ends of the solid Ca-axis. By this the function becomes uniquely defined over the whole solid calcium concentration range as shown in which enables use of equation (12) for the calculation of calcium migration.

After some initial numerical test the latter model gives better numerical stability then the solid calcium concentration formulation. Therefore, the equation which was ultimately selected and which introduces the variation of all physical parameters involved including advective transport is defined as:

$$\frac{\partial(\theta(c_{Ca,s}) \cdot c_{Ca,aq})}{\partial t} + \frac{\partial(\rho_b(c_{Ca,s}) \cdot K_d(c_{Ca,s}) \cdot c_{Ca,aq})}{\partial t} = \nabla \cdot \left(\theta(c_{Ca,s}) \cdot \xi(c_{Ca,s}) \cdot D_p \nabla c_{Ca,aq} \right) + \nabla \cdot \left(\vec{u} \cdot c_{Ca,aq} \right) \tag{14}$$

The Darcy velocity field is described by the vector variable   and diffusional change is determined by tortuosity ξ change.

3.2. Implementation of advective transport into continuum model with fractures

$$S \frac{\partial p}{\partial t} = \nabla \cdot \left(\frac{K_{mat}}{\rho_w \cdot g} \cdot \nabla p \right) \tag{15}$$

Where S, p, K_{mat}, ρ_w, and g are storage coefficient [1/Pa], fluid pressure [Pa], saturated hydraulic conductivity of the concrete matrix [m/s], water density [kg/m^3] and the gravitational acceleration constant [m/s^2], respectively. The Darcy's velocity vector $\vec{u}$ is then calculated as

$$\vec{u} = -K_{mat} \frac{\nabla p}{\rho_w \cdot g} \tag{16}$$

18
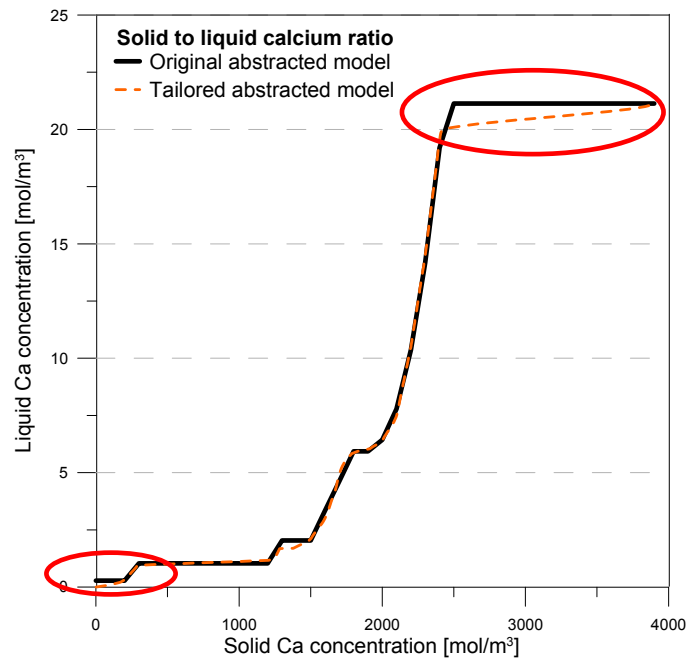
FIG. 5. Original and tailored abstracted model.
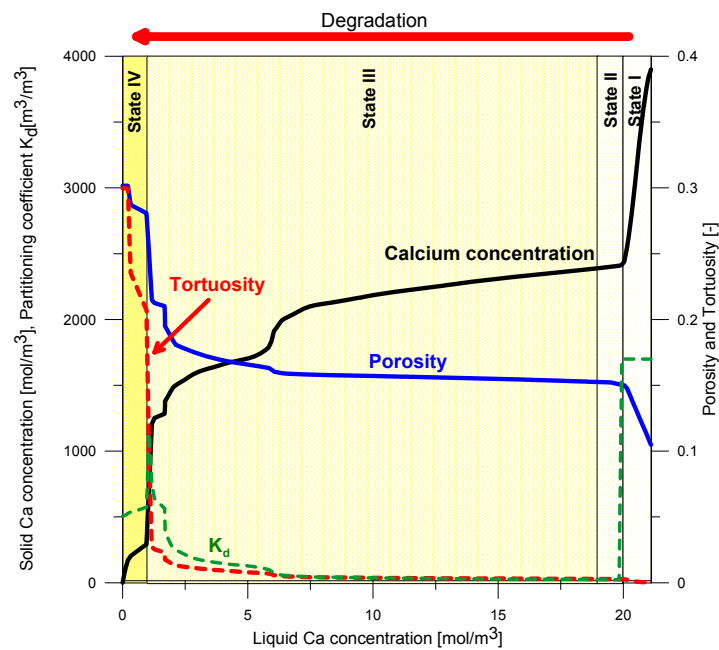
FIG. 6. Relationship between liquid and solid calcium. Also shown is the change in tortuosity and porosity as a result of continued cement leaching (degradation is from left to right).

Cracks may be modelled in two ways in the generic simulator COMSOL Multiphysics. The first approach is to explicitly express cracks as a geometrical property. This approach is fine if the crack is relatively wide and if the number of cracks is small. On the other hand, thin cracks would result in enormous computational resources owing to the fine discretization. The second approach, the so-called implicit formulation, is based on including a 1D (line) element into the 2D model. In this way, the discretization of the crack is only made in one dimension, whereas the majority of the remaining

domain does not need to be too finely discretized. The advantages of the implicit formulation are i) easier discretization, ii) better numerical stability, iii) higher computational efficiency and iv) an easy adaption to different crack dimensions. A possible drawback of this method is the decrease in transparency as concerns its implementation due to the mathematical manipulations involved in transformation of basic equation into a boundary formulation. Nevertheless, the computational efficiency is prioritized in our case because of the relative large number of fractures modelled.

Flow in cracks is modelled similarly to modelling flow in a porous matrix based on equation (15). Because the crack is modelled as a 1D element, crack dimension d_{crack} is added to ensure dimensional consistency between the porous matrix and the cracks:

$$S \cdot d_{crack} \cdot \frac{\partial p}{\partial t} = \nabla \cdot \left(d_{crack} \cdot \frac{K_{frac}}{\rho_w \cdot g} \cdot \nabla p \right),$$

(17)

In the crack formulation (eq. (18)) the storage coefficient S in both cases is put to a very low number representing water compressibility, which makes equations (15) and (17) almost represent steady-state. The Darcy velocity in the fracture is calculated as in equation (15), but by using tangential derivatives on the boundary instead of field pressure derivatives. Equation (17) is implemented in a weak form, which transforms domain integrals to the boundary ones. Equation (17) is multiplied by a test function $T*$ and integrated by parts:

$$0 = \int_\Omega T^* \cdot S \cdot d_{crack} \cdot \frac{\partial p}{\partial t} + \int_\Omega T^* \cdot \nabla \cdot \left(-d_{crack} \cdot \frac{K_{frac}}{\rho_w \cdot g} \cdot \nabla p \right)$$

$$0 = \int_\Omega T^* \cdot S \cdot d_{crack} \cdot \frac{\partial p}{\partial t} d\Omega - \int_\Gamma \left(T^* \cdot d_{crack} \cdot \frac{K_{frac}}{\rho_w \cdot g} \cdot \nabla p \right) \cdot \vec{n} \, d\Gamma + \int_\Omega \nabla T^* \cdot d_{crack} \cdot \frac{K_{frac}}{\rho_w \cdot g} \cdot \nabla p d\Omega$$

(18)

,

where Ω and Γ represent domain and boundary, respectively and $\vec{n}$ is outward normal to the boundary. Hydraulic conductivity K_{frac} of fractures is approximated by the formulation of Walton and Seitz [40] which assumes Poiseulle's flow between two parallel plates. The derivation results in the following notation for hydraulic conductivity of a single crack:

$$K_{frac} = \frac{\rho_w \cdot g \cdot b}{12\mu}.$$

(19)

The fracture aperture is denoted by b [m] and dynamic viscosity of water by μ [Pas]. Studies showed that the actual hydraulic conductivity is actually one- to two- thirds of the one based on equation (19). Similarly to the procedure in Walton and Seitz [40] one half is of the value from equation (13) is therefore used here:

$$K_{frac} = \frac{\rho_w \cdot g \cdot b}{24\mu}.$$

(20)

Transport equation (5) has to be rewritten in the non-conservative form when dealing with implicit fractures. Because the field variables interpret fractures as a source/sink boundary line, the velocity divergence is not zero which leads to spurious mass generation. Avoiding the use of velocity divergence as written in equation (21) solves this problem:

$$\frac{\partial}{\partial t}\left(\theta \cdot \frac{c_{Ca,s}}{K_d} + \rho_b \cdot c_{Ca,s}\right) = \nabla \cdot \left(\theta \cdot \xi \cdot \frac{D_p}{K_d}\nabla c_{Ca,s}\right) + \frac{\vec{u}}{K_d}\nabla c_{Ca,s}. \tag{21}$$

3.3. Numerical example

The example taken forward in this paper represents a two-layer concrete structure with different mechanical properties resulting in a different fracture network (FIG. 7). The example fracture network evolves from a concrete with only a few fractures (low fracture density) to a much more degraded concrete with a more intense fracture network (high fracture density). The assumption for the first network is that the top layer has one through-going fracture every m with an aperture of 300 µm. The second layer has one fracture at the top and bottom, but not throughgoing (10 cm deep) and with and identical aperture of 300 µm. This represents the fracture network at early time when the concrete degradation is still negligible.

A second fracture network exists at later time when the concrete degradation has become more severe owing to rebar corrosion, drying shrinkage, possibly earthquakes, etc.. In the first layer, 18 additional 10-cm deep fractures exist, all having an aperture of 300 µm. The second layer now has 20 10-cm deep fractures at its top and bottom, all 300 µm aperture.

It is assumed that the transition from the low to the high fracture density occurs after approximately 350 years. The effect of this increased fracture density on water flow, Ca leaching, and updating of hydraulic and transport properties will be included in the simulation.
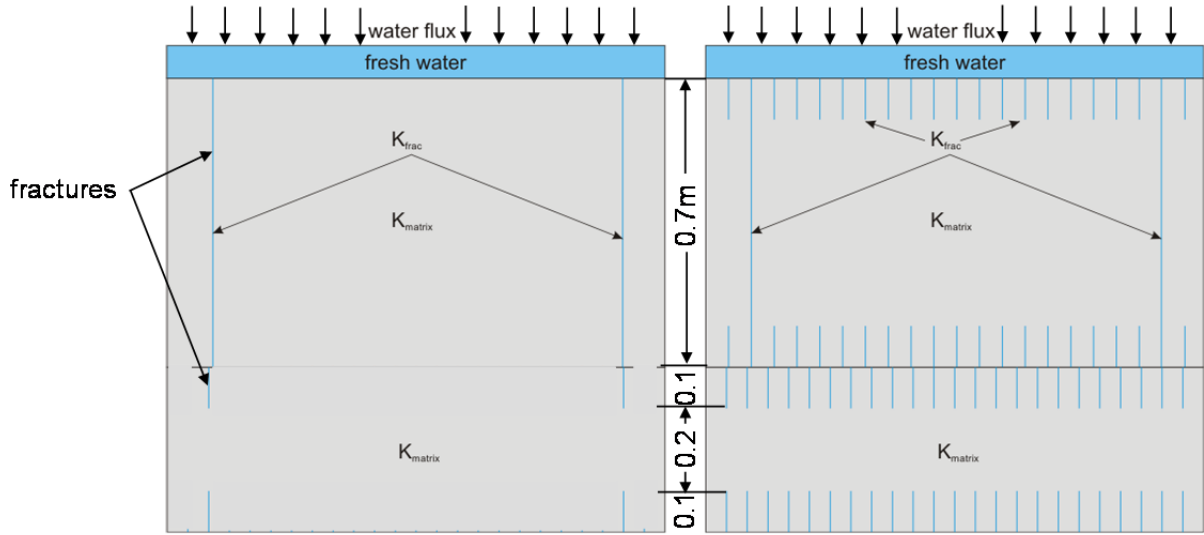
FIG. 7. Conceptual model for fractured concrete component. Low fracture density (left), high fracture density (right).

Water flow is defined by top and bottom constant pressure boundary conditions. Bottom boundary is arbitrarily set to zero pressure, while the top boundary respects the gradient $p = \rho_w \times g \times z_{top}$ [Pa], where z_{top} is the height of the model domain. Both vertical boundaries are defined by Neumann boundary condition. Initially the pressure inside is distributed as $\rho \times g \times z$. Concentration is defined only at the top

with the minimum value of solid calcium concentration 0.22 mol/kg. All other boundaries are no-flux Neumann boundary conditions. The initial concentration is the solid calcium concentration in concrete, which equals 3.89 mol/kg.

3.4. Modelling results

The numerical simulation focuses on the effect of different fracture networks on chemical concrete degradation. The level of chemical degradation can be studied in terms of the change in different hydraulic and transport properties (see section 2). Since the overall water permeability is one of the most important factors when addressing concrete degradation, this property is given as an indicator of overall degradation. Another indicator of the degree of concrete degradation is the total amount of Ca, which can be linked to one of the four states of cement degradation (section 1.3). The spatial distribution of the chemical degradation state will be displayed on the basis of the 2D model.

Initially, the concrete is intact and water flux through the porous matrix is very low. The degradation process is diffusion driven and progresses strictly from the top downwards. Due to the higher conductivity of fractures, water accumulates in the fractures and degradation progresses first in the vicinity of the water-filled fractures (FIG. 8). At the same time, a more uniform degradation front developes from the top of the concrete block. While the initial rate of degradation in the matrix concrete in absence of fractures is very slow, switching to the high density fracture network after 350 y accelerates the degradation rate. Because the number of throughgoing fractures in the top layer has not increased after 350 y, there remain relatively large zones of intact concrete characterized by a high Ca concentration and high pH (state I or II).

The combined effect of a more dense fracture network, calcium leaching and hydraulic and transport property updating in agreement with formulations described in section 2, on the water flux through the concrete block is shown in FIG. 9. The magnitude of the relative increase depends on parameters such as the initial matrix hydraulic conductivity, the number of throughgoing fractures, etc. The time frame within which the flux (i.e. hydraulic conductivity) increase occurs is very much mass balance driven: the more Ca present in the system, in terms of portlandite and CSH phases, the longer it takes to degrade the concrete for a given type of infiltrating water and for a given fracture network.
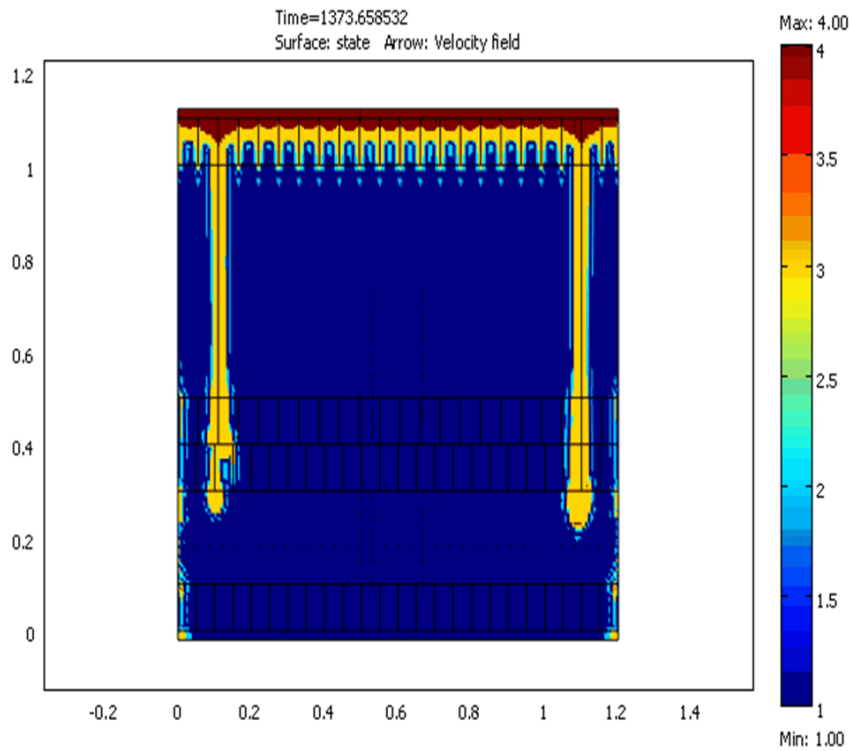
FIG. 8. Reactive transport calculation of water infiltration, cement mineral dissolution, and dynamic updating of hydraulic parameters. Results shown water infiltrating mainly along fractures, with associated cement dissolution after ~ 1400 years. Colours represent cement degradation state: I = undegraded (pH > 12.5), II = pH 12.5, III = 10 < pH < 12.5, IV = pH < 10.5.
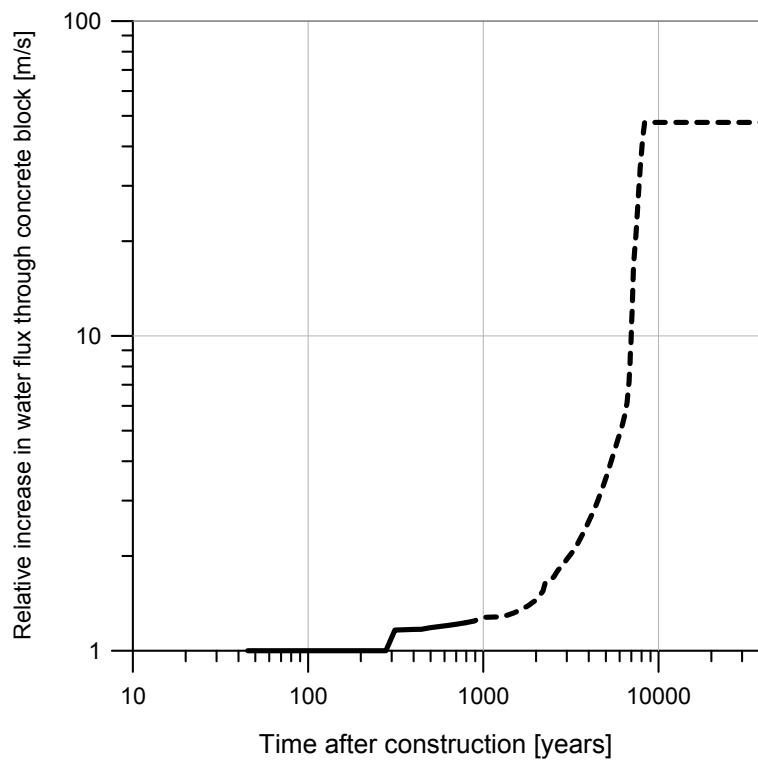
FIG. 9. Calculated relative increase in water flux through concrete block as a result of calcium leaching and subsequent hydraulic and transport property updating.

The reactive transport model also automatically updates the distribution ratios (R_d) in the whole 2D domain depending on the degradation state. Typical R_d values for state II and III are listed in TABLE 5; in most cases sorption in state III has not decreased compared to state II because sorption mainly takes place on CSH phases [1]. The model is thus also able to calculate the integrated effect of physical (flow) and chemical (transport) evolution on radionuclide migration.

TABLE 5. EVOLUTION OF DISTRIBUTION RATIO R_D AS FUNCTION OF CEMENT DEGRADATION STATE [1]

Element	State (II)	State (III)		Element	State (II)	State (III)
		Sorption on benchmark cement paste				
Am (+III)	***	≈		Pa (+IV)	****	≈
C (+IV)	***	≈		Pu (+IV)	****	≈
Cl (-I)	*	≈		Ra (+II)	**	≈
Cs (+I)	*	↑		Se(+IV)	**	≈
I (-I)	*	↓		Sr (+II)	*	≈
Nb (+V)	****	≈		Tc (+VII)	(*)	≈
Ni (+II)	**	≈		Th (+IV)	****	≈
Np (+IV)	****	≈		U (+IV)	****	≈

(*) $R_d < 10$ l/kg   * $R_d = 10\text{-}100$ l/kg   ** $R_d = 10^2\text{-}10^3$ l/kg   *** $R_d = 10^3 - 10^4$ l/kg   **** $R_d > 10^4$ l/kg

3.5. Conclusion

A 2D reactive transport model was developed in COMSOL that accounted for Ca leaching from concrete structures that had an evolving fracture network. The dissolution of calcium minerals from concrete resulted in a porosity increase and thus in an increase in hydraulic conductivity. The water flux through the concrete block consequently increased over nearly two orders of magnitude. Simulations with the 2D model also showed the heterogeneous nature of the calcium leaching process and the existence of nearly all major concrete degradation states across the concrete block. Leaching mainly occurred around the fractures, whereas unfractured matrix domains showed much less degradation and kept their high pH, high Ca concentration and low hydraulic conductivity for a much longer period. Although the chemical component of the model is very much simplified compared to the full-scale cement model discussed in section, it captures the main chemical concrete degradation processes and thus provides an effective tool to assess the evolution of physical and chemical characteristics of full-scale concrete structures. Fracture networks, either measured or postulated, can easily be accommodated in the model.

REFERENCES

[1] WANG, L., MARTENS, E., JACQUES, D., DE CANNIÈRE, P., BERRY, J., MALLANTS, D., Review of sorption values for the cementitious near field of a near surface radioactive waste disposal facility, NIROND-TR 2008-23 Version 1 (2008).

[2] GLASSER, F.P., MARCHAND, J., SAMSON, E., Durability of concrete – Degradation phenomena involving detrimental chemical reactions, Cem. Concr. Res. 38 (2008) 226-246.

[3] NEALL, F.B., Modelling of the near-field chemistry of the SMA repository at the Wellenberg site, PSI-Bericht Nr. 94-18 (1994).

[4] NEALL, F.B., Modelling the long-term chemical evolution of cement-groundwater systems, Mat. Res. Soc. Symp. Proc., 412 (1996) 483-490.

[5] BERNER, U., Evolution of pore water chemistry during degradation of cement in a radioactive waste repository environment, Waste Manag. (1992), 12, 201-219.

[6] ATKINSON, A., EVERITT, N.M., GUPPY, R., Evolution of pH in a radwaste repository: Experimental simulation of cement leaching: Part 1, DOE/RW/89/025 (1989).

[7] ATKINSON, A., EVERITT, N.M., GUPPY, R., Evolution of pH in a radwaste repository: Internal reactions between concrete constituents: Part 2, DOE/RW/89/025 (1989).

[8] MORANVILLE, M., KAMALI, S., GUILLON, E., Physicochemical equilibria of cement-based materials in aggressive environments – experiment and modeling, Cem. Concr. Res. 34 (2004) 1569-1578.

[9] JACQUES, D., MALLANTS, D., Modelling the potential and actual evapotranspiration and drainage at the nuclear zone Mol-Dessel, NIROND-TR 2008-25 Version 1 (2008).

[10] LOTHENBACH, B., WINNEFELD, F., Thermodynamic modeling of he hydration of Portland cement, Cem. Concr. Res. 36 (2006) 209-226.

[11] LOTHENBACH, B., MATSCHEI, T., MÖSCHNER, G., GLASSER, F.P., Thermodyanmic modeling of the effect of temperature on the hydration and porosity of Portland cement, Cem. Concr. Res. 38 (2008) 1-18.

[12] MATSCHEI, T., LOTHENBACH, B., GLASSER, F.P., Thermodynamic properties of Portland cement hydrates in the system CaO-Al2O3-SiO2-CaSO4-CaCO3-H2O, Cem. Concr. Res. 37 (2007) 1379-1410.

[13] HUMMEL, W., BERNER, U., CURTI, E., PEARSON, F.J., THOENEN, T., Nagra/PSI chemical thermodynamic data base 01/01, Universal Publishers/uPUBLISH.com, USA (2002).

[14] KULIK, D.A., GEMS-PSI 2.2, PSI-Villigen, Switzerland, http://gems.web.psi.ch (2007).

[15] JOHNSON, J.W., OELKERS, E.H., HELGESON, H.C., SUPCRT92: A software package for calculating the standard molal thermodynamic properties of minerals, gases, aqueous species and reactions from 1 to 5000 bar and 0 to 1000°C, Comp. and Geosci., 18 (1992) 899-947.

[16] PARKHURST, D.L., APPELO, C.A.J., User's guide to PHREEQC (version 2) – A computer program for speciation, batch-reaction, one-dimensional transport, and inverse geochemical calculations, Water-Resources Investigation Report 99-4259, Denver, Colorado (1999).

[17] JACQUES, D., Benchmarking of the cement model and detrimental chemical reactions including temperature dependent parameters. NIROND-TR 2008-30 Version 1 (2008).

[18] BROUWERS, H.J.H., VAN EIJK, R.J., Alkali concentrations of pore solution in hydrating OPC, Cement Concrete Res., 33 (2003) 191-196.

[19] JACQUES, D., WANG, L., MARTENS, E., MALLANTS, D., Time dependence of the geochemical boundary conditions for the cementitious engineered barriers of the Belgian surface disposal facility. NIROND-TR 2008-24E (2008).

[20] NEIRYNCK, J., GENOUW, G., COENEN, S., ROSKAMP, P., Depositie en luchtkwaliteit in Vlaamse bosgebieden, Instituut voor bosbouw & wildbeheer, mededelingen 2004-1 (2004).

[21] BROOK, G.A., FOLKOFF, M.E., BOX, E.O., A World model of soil carbon dioxide, Earth Surf. Proc. and Landsforms 8 (1983) 79-88.

[22] UBA, Manual on methodologies and criteria for modelling and mapping critical loads & levels and air pollution effects, risks and trends, http://www.icpmapping.org (2004).

[23] DE VRIES, W., Soil Response to acid deposition at different regional scales, Field and laboratory data, critical loads, and model predictions, Doctoral thesis, Agricultural University, Wageningen, the Netherlands, (1994).

[24] APPELO, C.A.J., POSTMA, D., Gechemistry, groundwater and pollution, 2nd edition, A.A. Balkema Publishers (2005).

[25] HANSEN, B.K., POSTMA, D., Acidification, buffering, and salt effects in the unsaturated zone of a sandy aquifer, Klosterhede, Danmark, Water Resour. Res., 31 (1995) 2795-2809.

[26] GLASSER, F.P. Application of inorganic cements to the conditioning and immobilisation of radioactive wastes. In: Handbook of advanced radioactive waste conditioning technologies, Ed. M.I. Ojovan. pp. 67-135, Woodhead, Oxford (2011).

[27] PFINGSTEN, W., SHIOTSUKI, M., Modeling a cement degradation experiment by a hydraulic transport and chemical equilibrium coupled code, Material Research Society Symposium Proceedings, 506 (1998) 805-812.

[28] GALINDEZ, J.M., MOLINERO, J., SAMPER, J., YANG, C.B., Simulating concrete degradation processes by reactive transport models, J. Phys IV France 136 (2006) 177-188.

[29] VAN DER LEE, J., DE WINDT, L., LAGNEAU, V., Application of reactive transport models in cement-based porous media, Concrete Modelling '08 (Eds. E. Schlangen, G. De Schutter), May 26-28 2008, Delft, RILEM Publications (2008) 463-470.

[30] JACQUES, D., ŠIMŮNEK, J., VAN GENUCHTEN, M.Th., MALLANTS, D., Operator-splitting errors in coupled reactive transport codes for transient variably saturated flow and contaminant transport in layered soil profiles, Journal of contaminant hydrology 88 (2006) 197-218.

[31] JACQUES, D., ŠIMŮNEK, J., VAN GENUCHTEN, M.Th., MALLANTS, D., Coupling hydrological and chemical processes in the vadose zone: A case study on long term uranium migration following mineral P-fertilization, Vadose Zone Journal 7 (2008) 698-711.

[32] JACQUES, D., ŠIMŮNEK, J., VAN GENUCHTEN, M.Th., MALLANTS, D., Detailed modeling of coupled water flow, solute transport and geochemical reactions: Migration of heavy metals in a podzol soil profile, Geoderma 145 (2008) 449-461.

[33] JACQUES, D., WANG, L., MARTENS, E., MALLANTS, D., Modelling chemical degradation of concrete during leaching with rain and soil water types, Cement and Concrete Research 40 (2010) 1306-1313,doi:10.1016/j.cemconres.2010.02.008 (2010).

[34] MALLANTS, D., VAN GENUCHTEN, M.Th., ŠIMŮNEK, J., JACQUES, D., SEETHARAM, S., 2010. Leaching of contaminants to groundwater – Chapter 18. In (F.Swartjens, Editor) Dealing with Contaminated Sites. From Theory towards Practical Application, ISBN 978-90-481-9756-9, Springer Verlag, Dordrecht, The Netherlands, 2010, pp. 787-850, DOI: 10.1007/978-90-481-9757-6_1.

[35] WISSMEIER, L., BARRY, D.A., Effect of mineral reactions on the hydraulic properties of unsaturated soils: Model development and application, Advances in Water Resources, 32 (2009) 1241-1254.

[36] GARBOCZI, E.J., BENTZ, D.P., Computer simulation of the diffusivity of cement-based materials, Journal of Material Science, 27 (1992) 2083-2092.

[37] ŠIMŮNEK, J., ŠEJNA, M., SAITO, H., SAKIA, M., VAN GENUCHTEN, M.Th., The HYDRUS-1D Software Package for Simulating the Movement of Water, Heat, and Multiple Solutes in Variably Saturated Media, Version 4.08, HYDRUS Software Series 3, Department of Environmental Sciences, University of California Riverside, Riverside, California, USA (2008).

[38] JACQUES, D., ŠIMŮNEK, J., Notes on HP1 – a software package for simulating variably-saturated water flow, heat transport, solute transport and biogeochemistry in porous media, HP1 Version 2.2, SCK•CEN-BLG-1068 (2010).

[39] COMSOL Multiphysics, User's guide (Version 3.5a), COMSOL AB (2009).

[40] WALTON, J.C., SEITZ, R.R., Performance of intact and partially degraded concrete barriers in limiting fluid flow, NUREG/CR-5614. EGG-2614 (1991).